

Planar radial extension for constitutive modeling of anisotropic biological soft tissues

Madhavan L. Raghavan¹, Kathleen Lin^a, Manasi Ramachandran^a, Aleko Nadareishvili^a, Ryan Amelon^a, and Jia Lu^b

^aBiomedical Engineering, University of Iowa, Iowa City, IA 52242

^bMechanical Engineering, University of Iowa, Iowa City, IA 52242

Abstract

Characterizing the mechanical properties of anisotropic biological soft tissues poses unique challenges. One among these challenges is the lack of *a priori* information on the underlying fiber orientations that drive its anisotropic behavior. While fiber orientations in very thin planar tissues may be characterized by non-destructive means prior to mechanical testing, this is not possible with thick tissues. A planar radial extension test of circular planar biological soft tissue specimen is proposed for simultaneously ascertaining both the preferred fiber orientations and the mechanical properties. When pulled by a radial load, a circular specimen will deform into an elliptical shape revealing its stiffest direction (minor axis of ellipse) and its anisotropic properties. Numerical investigations were used to assess the stress and strain fields generated and justify the analytical equations to calculate stress and strain. A simple manual force-controlled planar radial extension device was constructed. A porcine aortic specimen was subjected to planar radial extension testing and the test data was fit to an anisotropic finite strain constitutive model to demonstrate the feasibility of this method for assessment of anisotropic biological soft tissues whose material symmetry is not known *a priori*.

1. Introduction

Planar biological soft tissues – tissues with a low thickness compared to other dimensions – abound in the human body. Blood vessels, skin, intestinal walls, urinary bladder, and heart valves may be thought of as planar biological soft tissues. Determining the material properties of these presumably anisotropic tissues can aid in understanding and modeling their mechanics in living systems. Traditionally, anisotropic planar tissues are mechanically tested by orthogonal biaxial extension of square specimens followed by estimation of parameters of a chosen finite elastic constitutive model [1]. Here, assuming the material is comprised of two orthogonal families of fibers, the material axes are aligned with the orthogonal test axes for extension testing. Where in-plane shear properties are to be characterized, and where the test equipment is appropriately equipped, the material axes may be aligned oblique to the test axes resulting in in-plane shear stress and/or strain fields under extension [2]. For these orthogonal extension tests to be of value, *a priori* knowledge of material fiber directions in the specimen to be tested is highly desired. Unlike man-made materials, where the material fiber-direction is pre-determined by design, they may be unknown in biological materials. Further, ascertaining these fiber orientations by non-mechanical means can be quite challenging. Optical methods have been reported for identification of structural fiber orientations in thin biological tissues (less than half millimeter) such as heart valve leaflets [1], but rarely in thick tissues such as arteries because optical methods are not as effective with thick tissues. Indeed, among reported biaxial orthogonal tests of thick biological soft tissues, material axes were understandably presumed to be oriented along test axes [3, 4]. The same limitation of having to know material fiber orientations *a priori* exists in inflation testing of conduit-like structures as well, where too, a presumption that the preferred orientation is either circumferential or axial is rendered inevitable [5]. In thick planar biological soft tissues, the lack of *a priori* knowledge of material fiber orientation therefore limits the accuracy of results from the traditional orthogonal biaxial extension tests. The limitation is likely aggravated in structures that are not necessarily cylindrical (e.g., aortic arch) or those afflicted by pathology (e.g., aortic aneurysms) where assumptions on fiber orientations are more questionable.

We submit that planar radial extension testing (PRET) of a thick circular soft tissue specimen will reveal the underlying preferential orientations (if any) of material fibers while also allowing for estimation of finite elastic model parameters

¹Corresponding author . Email: ml-raghavan@uiowa.edu

obviating the need for *a priori* knowledge of fiber structure. Nielsen et al. (2002) [6] first reported on such multiaxial tests to study inhomogeneous isotropic properties of elastic rubber membranes and later reported using similar test methods for characterization of anisotropic skin tissue [7]. Here, we built a simple apparatus for subjecting circular planar tissue specimens to radial extension, performed numerical simulations of PRET to assess whether a homogeneous strain field may be induced under realistic test conditions, performed a demonstrative test on a planar biological soft tissue and estimated its stiffest direction and anisotropic material parameters for a finite elastic constitutive model.

2. Methods

2.1 Concept of planar radial extension testing (PRET)

The underlying principle of PRET is that material symmetry and mechanical properties of a planar tissue can be phenomenologically inferred if it is simultaneously pulled (force-control) or stretched (displacement control) in all planar directions (i.e., radially) while measuring the deformation or force field respectively. A force controlled PRET involves applying the same force all around the circumference of the circular specimen and studying the deformed shape. If the specimen becomes elliptical, then the minor axis of the ellipse is its stiffest direction. This method allows direct visual identification of material symmetry, but has precision related challenges because the deviation of specimen shape from a circle may only be perceivable at large deformations. The displacement controlled PRET involves subjecting the circular specimen to constant displacement around its perimeter such that the circular shape is maintained; the material symmetry is inferred by studying the distribution of force around its perimeter that was required to maintain the circular shape under deformation. The axis along which the force is highest is the stiffest direction. The advantage of this method is its high precision. Even under very small displacements, the material symmetry may be inferred, but it does not allow for direct visualization of anisotropy, may have some non-circular deformation away from the pins, and requires computer-control for reliable low-scale extensions and accurate measurement of forces at the points of extension.

Theoretically, for true radial extension, the circular specimen will need to be pulled at an infinite number of points. But from a practical standpoint, gripping constraints require that the circular specimen be pulled radially at a finite number of points. With a 'sufficient' number of pull-points for a 'large enough' specimen, the stress concentrations at the gripping points could subside and result in a region at the center with a homogeneous stress/strain field where markers may be placed for strain field measurement.

Figure 1 illustrates force-controlled PRET of a circular specimen stretched using 16 finite suture points.

2.2 Numerical investigation of edge-effects on stress and strain fields

The feasibility of the proposed planar radial extension test rests on precision-related considerations that need to be investigated before embarking on building the test apparatus. Specifically, it is vital to examine whether the edge effects subside within a short enough distance from the force points and result in a large enough homogeneous strain field for placement of markers. Numerical simulation of PRET of a circular specimen with dimensions and material behavior reflecting that of a porcine aorta was performed to gain insights into such issues and assess its feasibility. The porcine aorta is a 1.5 cm diameter tubular vessel from which a circular 3 cm diameter specimen may be easily obtained (as shown in

Figure 1 A-D). A finite element model of a 3 cm diameter circular specimen was constructed using 1714 triangular plane stress elements (CPS3 - ABAQUS, Dassault Systèmes Simulia Corp., Providence, RI). A finite elastic orthotropic constitutive model previously reported by Fung and colleagues [8] and widely used for modeling aortic tissue was used to characterize material behavior [9]. The Fung model is described by an orthotropic exponential form of strain energy density function,

$$W = c \left(e^{[c_1 E_{11}^2 + c_2 E_{22}^2 + c_3 E_{11} E_{22} + c_4 E_{12}^2]} - 1 \right) \quad (1)$$

where, W is strain energy density; E_{ij} are the Green's strain tensor components for an orthotropic material with the stiff fiber aligned along the '1' direction; c , c_1 , c_2 , c_3 , and c_4 are material parameters that are estimated from experiments. For the simulation, we chose parameter values from our experiments (discussed subsequently). Nominal parameter values were also input for the coefficients associated with normal and shear strains for the 3rd dimension (E_{33} , E_{13} and E_{23} terms) in order to perform the analysis, but the findings should be mostly insensitive to these.

$c = 0.382 \text{ N/mm}^2$; $c_1 = 1.285$; $c_2 = 0.889$; $c_3 = 0.378$; $c_4 = 0.362$.

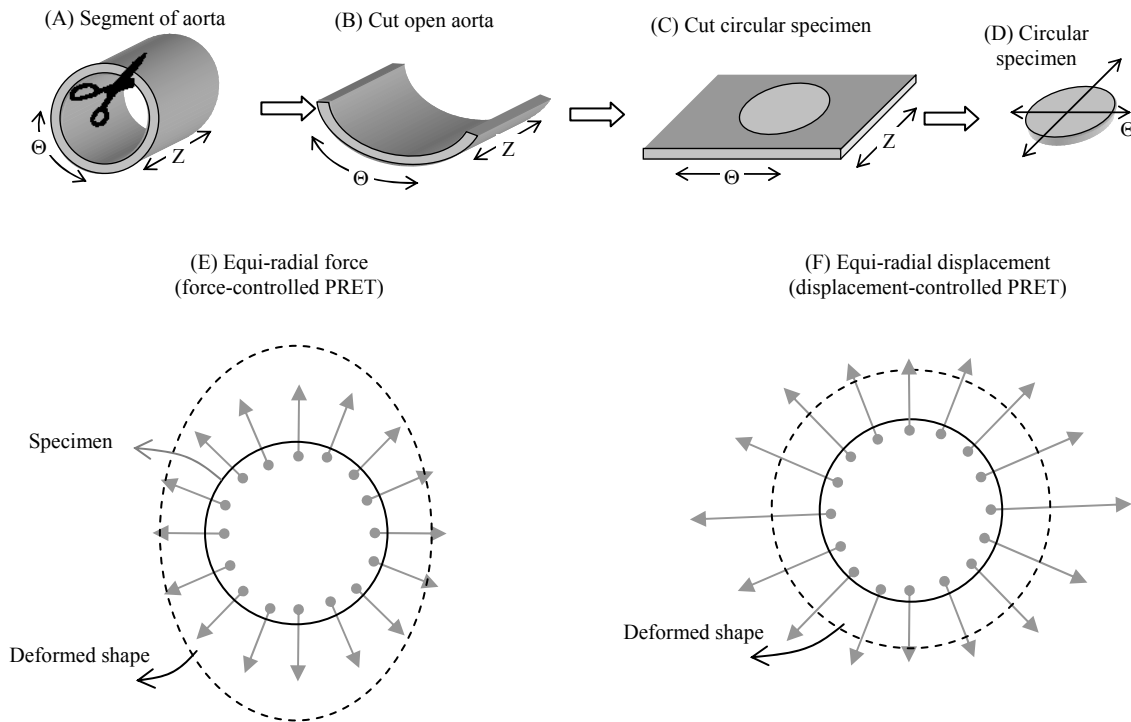


Figure 1. Conceptual illustration of PRET of a circular anisotropic specimen. (A) When pulled with equal force radially, the specimen will deform to an ellipse with the minor axis indicative of its stiffest direction; and (B) when pulled to induce equal displacement

The ratio, c_1/c_2 is a measure of the ratio between stiffness in the 1 direction (stiff fiber) to the stiffness in the 2 direction (cross-fiber or weak fiber). A radial force of 2.5 N was applied in each of 16 points, 0.3 cm from the periphery of the circular specimen precisely as shown in the illustration in Figure 2. The center node of the specimen was constrained in all degrees of freedom to suppress rigid body motion without affecting the results. ABAQUS was used for performing the analysis. The stiff fiber direction was set as the horizontal direction and the weak fiber direction as vertical (Figure 2A). The normal stress and strain along fiber directions were plotted. As expected, the circular specimen deformed to a perceptible elliptical shape with its minor axis precisely along the presumed fiber axis direction ('1' direction because parameter $c_1 > c_2$) as seen in Figure 2C&D. From the distribution of fiber stress and strain components, it is clear that the edge effects that peak at the force points at the radius of 1.2 cm, subside rapidly, resulting in a mostly homogenous field within a radius of 0.75 cm – half the radius of the specimen. Figure 2B illustrates this by plotting the stress components at all the nodes against their un-deformed radius. This suggests that markers need to be placed inside the perimeter of a 0.75 cm radius circle. The FE analysis was repeated with shell elements, and a very high level of anisotropy ($c_1/c_2=10$) in order to simulate a worst case scenario and here too, a homogeneous stress and strain field was found within half the radius of the specimen. This suggests that the size of the homogeneous stress and strain field is generally insensitive to the specific material parameters used. The results of the numerical investigation are consistent with the notion that edge effects will subside rapidly to result in a large enough region of homogenous stress/strain and serves as a proof-of-concept for PRET.

2.3 Design of a simple PRET apparatus

A simple manually operated PRET system was built to assess the practicalities and optimize design choices. This device, pictured in Figure 3, is capable of a force controlled PRET. This stage-1 device was fabricated using a 40" diameter circular block mounted on a table top as the base. A series of 16, 2" diameter pulleys were fixed along the periphery of this base, each 22.5° apart ($360^\circ/16$). Sixteen suture wires with connector pins to grip the specimen at one end and plastic containers for holding weights at the other end ran over the pulleys. Individual weight containers – not a single loading point – were needed here even if the loading is uniform radial traction because anisotropic specimens will deform obliquely causing some weights to drop more than others. If all suture wires were attached to a single weight, then some wires will become slack while others remain taut, thus affecting the ability to control load. A tripod fixed digital 3 MP camera was used directly above the specimen and whose images are used for measurement of the displacement field.

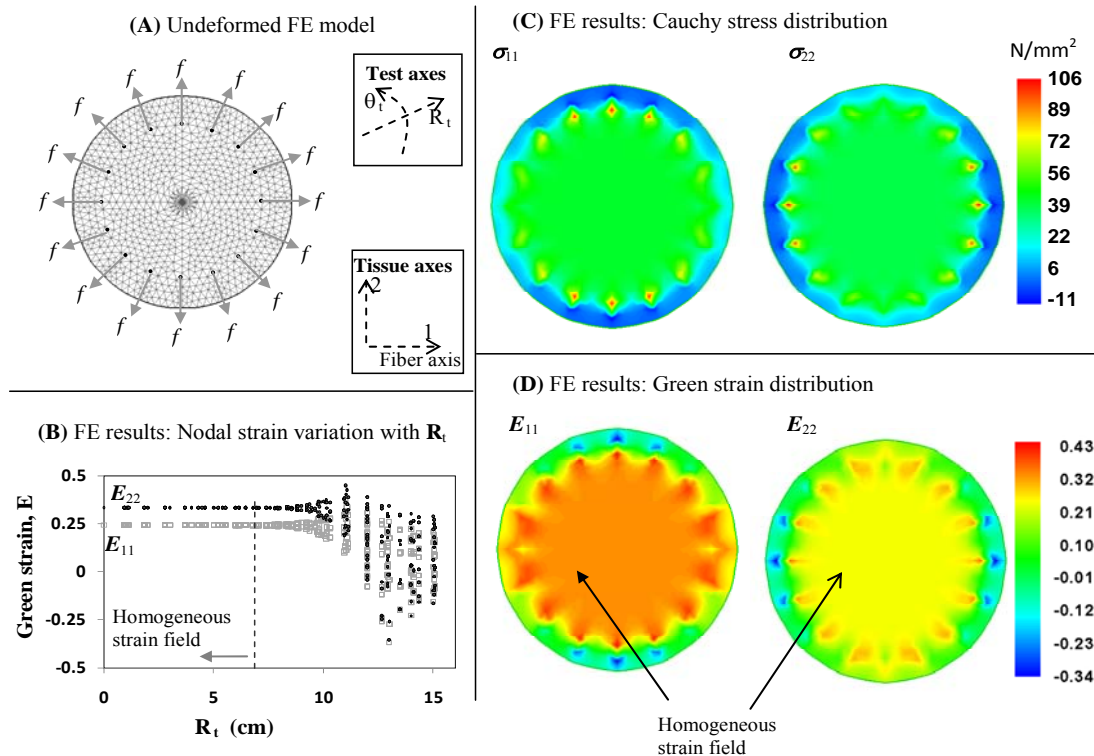


Figure 2. Numerical simulation of PRET of a circular specimen whose stiffest direction is along the horizontal direction (A). It is subjected to radial force, $F(R_t)$ of 4N at 16 points around its circumference (θ). All images (A, C and D) are to the same scale. Note that the circular specimen deforms into an elliptical shape with a minor axis precisely along the *a priori* stiffest direction. Further, the results show that the edge effects from the pull-points dissipate within a short distance resulting in a homogeneous stress and strain field (see B, C, and D). The markers may then be placed within the homogeneous field region of $R_t \leq 0.75$ cm (see C) – roughly for the first half of the total specimen diameter.

2.4 PRET of a porcine aorta

A freshly harvested porcine thoracic aorta was cut into a circular specimen, 3 cm in diameter using a die (

Figure 1 1A-D). The circumferential direction was marked using India ink before cutting. A pin insertion die was fabricated using which 16 exactly spaced holes were made in the specimen 2 mm from the edge (along a 2.6 cm diameter circle). Further, a circle of 0.75 cm radius was stamped on the specimen, so it may serve as a marker within the homogeneous strain region (as dictated by our numerical simulation). The 16 pins at one end of each of 16 suture wires were inserted into the specimen and run over the pulley. Figure 3 shows the apparatus at the zero load state (ignoring the negligible weight of the plastic container). The specimen was periodically squirted with saline to keep it moist during the entire duration of the test. The force at each of the suture points (f) was controlled by gradually placing precision machined 1.1 cm, 0.083N metal weights into the containers (see Figure 3).

To perform the force-controlled PRET, the specimen was subjected to roughly 0.314N (4 metal balls) increments of load (f) from 0 to 2.590N in each grip point: $f = 0\text{N}, 0.628\text{N}, 0.942\text{N}, 1.256\text{N}, 1.57\text{N}, 1.884\text{N}, 2.197\text{N}, 2.511\text{N}$ and 2.590N. The specimen was periodically squirted with saline during the test procedure. Three investigators were involved in gently placing of the metal balls into the containers in order to simultaneously load the specimen and minimize asymmetry during the loading process. Further, the lead balls were loaded incrementally to again minimize asymmetry of loading during the process. At each increment of load, the specimen was allowed at least 1 minute to equilibrate and then a photograph of the deformed specimen was taken using the overhead camera at each load increment. The loading was stopped when visible signs of the specimen damage at the suture point became apparent. The image data were digitized to extract the x-y coordinates of a finite number of points lying on the perimeter of the stamped marker (circular shape at zero load; increasingly elliptical at higher loads). These coordinates were transformed to polar coordinates, so that the displacement field may be expressed using the test axes, R_t and θ . The minor and major axes were identified and an ellipse was fit to determine the major and minor half-dimensions of the ellipse (a and b) for each load increment.

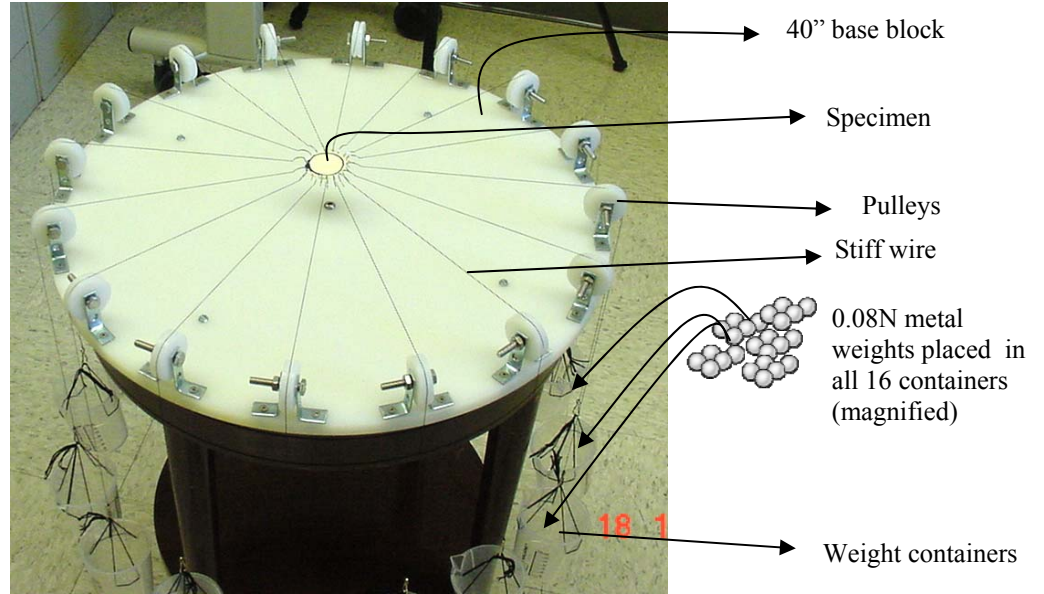


Figure 3. Photograph of a simple apparatus for force-controlled PRET. Weight containers hanging from stiff wires off of pulleys were loaded with lead weights to subject specimen to equi-radial force

2.5 Constitutive model parameter estimation

We fit the experimental data to the Fung-type exponential strain energy density function (Equation 1) without the E_{12} term as this is negligible in our experiment. Thus,

$$W = \frac{1}{2}c(e^Q - 1) \quad \text{with, } Q = c_1 E_{11}^2 + c_2 E_{22}^2 + 2c_3 E_{11}E_{22} \quad (2)$$

c and c_i are material parameters with 1 referring to the stiffest direction. The displacement field is,

$$x_1 = \lambda_1 X_1; \quad x_2 = \lambda_2 X_2; \quad x_3 = [1/(\lambda_1 \lambda_2)] X_3$$

where the stretch ratio across thickness (λ_3) is determined by assumption of incompressibility. When a and b are major and minor half-dimensions of ellipse, R is the radius of the marked circle (reference configuration), the relevant stretch ratios and Green strains are

$$\lambda_1 = a/R; \quad \lambda_2 = b/R; \quad E_{11} = \frac{1}{2}(\lambda_1^2 - 1); \quad E_{22} = \frac{1}{2}(\lambda_2^2 - 1) \quad (3)$$

Cauchy stresses at the homogeneous strain region of the specimen will be the traction at the boundary.

$$\sigma_{11} = \sigma_{22} = \frac{16f}{LH} \quad (4)$$

Where 16 is total number of pull-points, f is force at each pull-point, $H=1.5\text{mm}$ is the thickness of sample, and L is length of ellipse in current configuration calculated by Ramanujan's approximation:

$$L = \pi(3(a+b) - \sqrt{10ab + 3(a^2 + b^2)}) \quad (5)$$

The normal Cauchy stresses along fiber directions are:

$$\begin{aligned} \sigma_{11} &= c \lambda_1^2 (c_1 E_{11} + c_3 E_{22}) e^Q \\ \sigma_{22} &= c \lambda_2^2 (c_2 E_{22} + c_3 E_{11}) e^Q \end{aligned} \quad (6)$$

where, σ_{ii} , E_{ii} , λ_i , and Q are determinable using Equations (2), (3), (4) and (5) from the experimentally measured f , a , b , and H .

The major and minor half-dimensions of the near-ellipse marker on the specimen, a and b , were determined for each load by fitting the digitized marker to an ellipse equation using the nonlinear regression Levenberg-Marquardt least squares algorithm (Igor Pro, Wavemetrics). Subsequently, the Levenberg-Marquardt leastsquares algorithm was also used to fit Equation 6 to the experimentally obtained f - a , b data to estimate the material parameters, c , c_1 , c_2 and c_3 while constraining the parameters in the following manner to ensure convexity of the strain energy function [10]:

$$c > 0, \quad c_1 > 0, \quad c_2 > 0, \quad c_1 c_2 > c_3^2$$

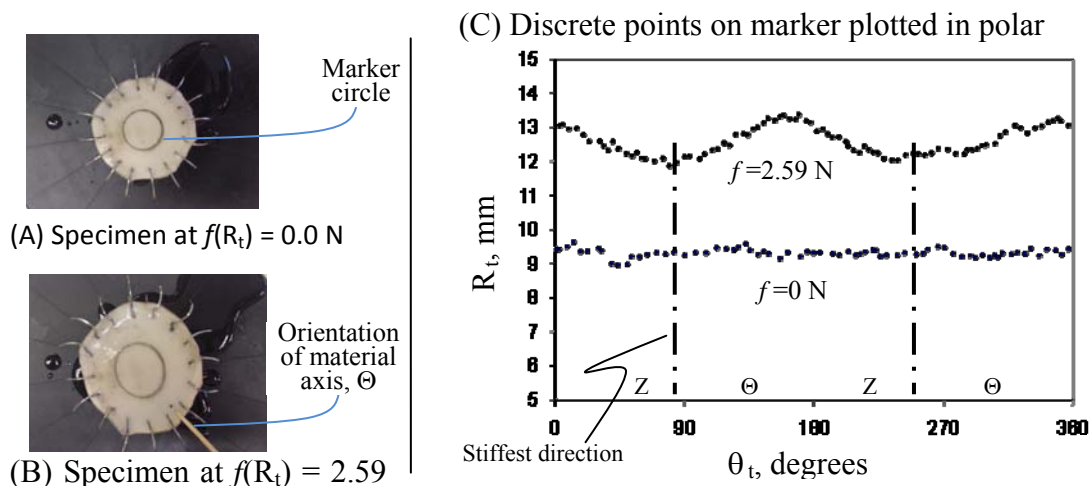


Figure 4. Results from PRET of aortic specimen to identify the preferred fiber direction. The images show how stamped circle on the specimen at $f=0$ N load deformed into an ellipse at $f=2.59$ N (images on same scale). The marking was digitized, converted to polar coordinates and the radius (R_t) of discrete points around the circumference was plotted as a function of circumferential location (θ). Note that at $f=0$ N, radius (R_t) is roughly constant around the circumference (θ) indicative of a circle while at $f=2.59$ N, there are clear minimas and maximas indicative of the minor and major axes of the ellipse relative to *in vivo* axes, Θ and Z. The stiffest direction and therefore preferred fiber direction corresponds closer to axial direction, Z (about 20 degrees from it) in this specimen.

3. Results

PRET of the aortic specimen showed a perceptible change in shape of the stamped marker from a circle at zero load to an ellipse under high loads. The specimen ‘failed’ (showed visual signs of tear at the pull points) beyond 2.59N. Figure 4 shows the specimen at the reference state and at the maximum load. Under visual observation and by analysis of images, it was clear that the circular specimen deformed into an ellipse with the major axis 20 deg. from circumferential direction (Θ) and the minor axis 20 degrees from the axial direction (Z) as seen in . Consequently, it is fair to infer that the preferred fiber orientation is 20 degrees to the axial direction. Figure 5 shows the digitized deformation of the circular marker for all loads as a plot of R_t versus θ_t , the test axes. For a circle, the radius (R_t) will remain unchanged with angle (θ_t), but for an ellipse, there will be a clear maxima and a minima for radius with angle. The gradual change of the circle to an ellipse is apparent in this figure. Additionally, since the aorta is a biological soft tissue, one would expect a large change in the amount of deformation at low loads (greater compliance) and less deformation at high loads (greater stiffness). This, too, is apparent in this graph where the largest change in average radius occurs between $f=0$ N and $f=0.628$ N – i.e., at the first increment of load. Fitting of ellipses to these shapes allowed for determination of the major and minor half-axes for each load, f (see Figure 6). The nonlinear regression of data shown in Figure 6 to Equation (5) converged to a good fit resulting in estimations of the material parameter values of the Fung-type constitutive model: $c = 0.382$ N/mm², $c_1 = 1.285$, $c_2 = 0.889$, $c_3 = 0.378$.

4. Discussion

Biological soft tissues present unique challenges during characterization of their mechanical properties unlike man-made synthetic constructs. Among them is the challenge of ascertaining the unknown material symmetry. Tissues that present with pathologies further aggravate this limitation as it makes assumptions on material symmetry more questionable. Unlike in the case of traditional orthogonal biaxial extension tests, a mechanical test method that does not impose the need to have *a priori* knowledge of underlying fiber structure can be quite valuable. We report precisely such a method here. In a series of remarkable reports on what they termed multiaxial tests, Nielsen and colleagues [6, 7, 11] have already reported on planar radial extension tests of rubber and skin tissue using a sophisticated computer controlled apparatus with 16 pull points. They studied heterogeneous isotropic and anisotropic tissues while estimating the material parameters using a reverse-FE optimization procedure.

In this proof-of-concept report, we demonstrate an experimental and analysis method for simultaneously estimating the material symmetry and mechanical properties of planar biological soft tissues. There are similarities with their method such as the number of pull points, etc. However, the method we report here is different from their

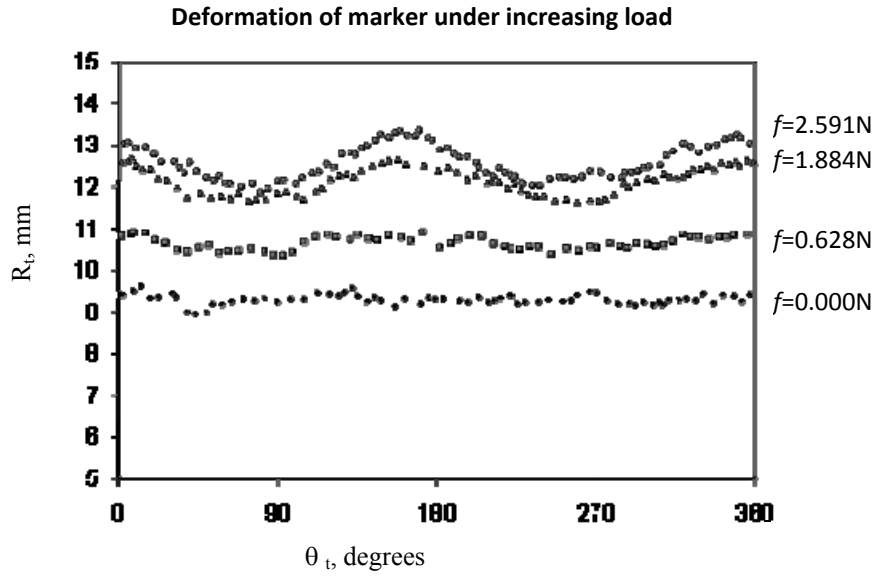


Figure 5. Test results demonstrating the evolving elliptical shape (maxima and minima of R_t) of the stamped marker from a circular shape (flat R_t) with increasing load. Note also the large change in average radius at low loads (between $f=0N$ to $f=0.628N$) and the low change at high loads indicative of the nonlinear stiffening characteristic of biological soft tissues.

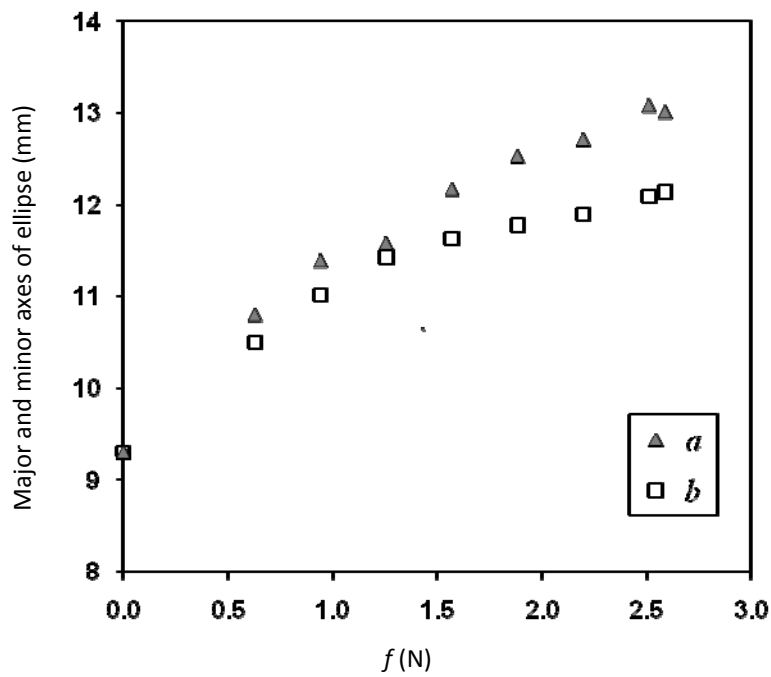


Figure 6. Major and minor axes of ellipse with increasing load

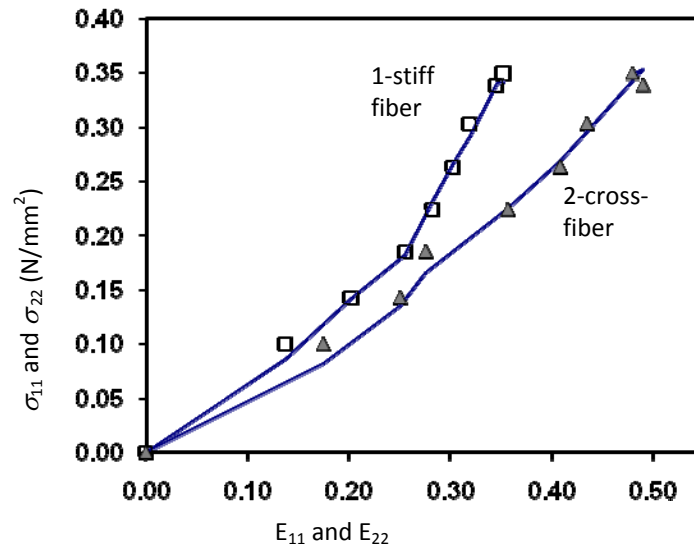


Figure 7. Fung-model curve fit to experimental data for estimation of parameters

approach in a few ways. The merits of this approach are that we use a simple and easily constructed test apparatus and do away with the need for reverse-FE based optimization by demonstrating that a homogeneous soft tissue will indeed have a large enough region of homogeneous stress and strain field that will permit direct estimation of material parameters using straightforward nonlinear regression. Reverse-FE based optimization can become problematic when multiple parameters are to be optimized and this limitation is avoided. But the current proposed approach is not without limitations. If the specimen is heterogeneous, the method of estimation we report here is likely not viable and a Nielsen type reverse-FE based approach does become inevitable, despite its limitations in terms of accuracy in estimations. The same is the case for small specimens where the edge effects may not subside to create a measurably large enough homogeneous strain field around the center of the specimen. Transmural variations in fiber orientations (if any) will likely not be captured using a PRET-based measurement. The current manual apparatus has some specific limitations such as the difficulties in preconditioning the specimen and the inability to perform creep/relaxation type testing. But these limitations are likely addressed by a computer-control PRET apparatus.

In the case of the aortic specimen we tested, we found that that the stiffest direction was neither circumferential nor longitudinal. There are conflicting findings on which among circumferential and axial directions are typically stiffer from biaxial studies with some suggesting circumferential [12] while others longitudinal [13]. Likely these differences depend on species and location, but nevertheless underscore the uncertainty surrounding material symmetry. This experiment is exploratory in nature and therefore more investigations may be needed to confirm the findings. But the current report does demonstrate the proof-of-concept underlying the planar radial extension test protocol and the feasibility of extracting the nature of anisotropy and the material parameters of a biological soft tissue whose material symmetry is not known *a priori*.

References

- Sacks, M.S., C.J. Chuong, and R. More, Collagen fiber architecture of bovine pericardium. *ASAIO J*, 1994. 40(3): p. M632-7.
- Sacks, M.S., et al., *In vivo three-dimensional surface geometry of abdominal aortic aneurysms*. *Ann Biomed Eng*, 1999. 27(4): p. 469-79.
- Nicosia, M.A., et al., *Biaxial mechanical properties of porcine ascending aortic wall tissue*. *J Heart Valve Dis*, 2002. 11(5): p. 680-6; discussion 686-7.
- Vande Geest, J.P., M.S. Sacks, and D.A. Vorp, *Age dependency of the biaxial biomechanical behavior of human abdominal aorta*. *J Biomech Eng*, 2004. 126(6): p. 815-22.
- Chuong, C.J. and Y.C. Fung, *Three-dimensional stress distribution in arteries*. *J Biomech Eng*, 1983. 105(3): p. 268-74.
- Nielsen, P.M., et al., *Instrumentation and procedures for estimating the constitutive parameters of inhomogeneous elastic membranes*. *Biomech Model Mechanobiol*, 2002. 1(3): p. 211-8.
- Kvistedal, Y.A. and P.M. Nielsen, *Investigating stress-strain properties of in-vivo human skin using multiaxial loading experiments and finite element modeling*. *Conf Proc IEEE Eng Med Biol Soc*, 2004. 7: p. 5096-9.

- Fung, Y.C., *Biomechanics : mechanical properties of living tissues*. 2nd ed. 1993, New York: Springer-Verlag. xviii, 568.
- Humphrey, J.D., *Cardiovascular solid mechanics : cells, tissues, and organs*. 2002, New York: Springer. xvi, 757.
- Wilber, J.P. and J.R. Walton, *The convexity properties of a class of constitutive models for biological soft tissues*. *Mathematics and Mechanics of Solids*, 2002. **7**(3): p. 217-235.
- Kvistedal, Y.A. and P.M. Nielsen, *Estimating material parameters of human skin in vivo*. *Biomech Model Mechanobiol*, 2009. **8**(1): p. 1-8.
- Doyle, J.M. and P.B. Dobrin, *Finite deformation analysis of the relaxed and contracted dog carotid artery*. *Microvasc Res*, 1971. **3**(4): p. 400-15.
- von Maltzahn, W.W., R.G. Warriyar, and W.F. Keitzer, *Experimental measurements of elastic properties of media and adventitia of bovine carotid arteries*. *J Biomech*, 1984. **17**(11): p. 839-47.